# Effects of continuously changing inlet wind direction on near-to-far wake characteristics behind wind turbines over flat terrain

Uchida, Takanori
Research Institute for Applied Mechanics(RIAM), Kyushu University

Gagnon, Yves
Universite de Moncton



出版情報：Journal of Wind Engineering & Industrial Aerodynamics. 220, pp.104869-, 2022-01. Elsevier
バージョン：

Journal of Wind Engineering & Industrial Aerodynamics 220 (2022) 104869

Contents lists available at ScienceDirect

Journal of Wind Engineering & Industrial Aerodynamics

journal homepage: www.elsevier.com/locate/jweia

# Effects of continuously changing inlet wind direction on near-to-far wake characteristics behind wind turbines over flat terrain

Takanori Uchida [a,*], Yves Gagnon [b]

[a] Research Institute for Applied Mechanics (RIAM), Kyushu University, 6-1 Kasuga-kouen, Kasuga, Fukuoka, 816-8580, Japan
[b] Universite de Moncton, 165 Hébert Boul, Edmundston, NB, E3V 2S8, Canada

ARTICLE INFO

*Keywords:*
Wind turbine wakes
Wind tunnel experiment
Large-eddy simulation (LES)
Actuator line (AL) model
Continuously changing wind direction

ABSTRACT

The wake characteristics of a utility-scale wind turbine under realistic atmospheric boundary layer conditions are affected by the continuously changing wind direction arriving at the wind turbine. In the present study, the effects of continuous changes in the incoming wind direction were studied for a wind turbine on flat terrain, with the objective of understanding the wake characteristics of the wind turbine. Thus, understanding the effects of continuously changing incoming wind direction on the wake characteristics of wind turbines over flat terrain is important in the design of wind farm layouts, including in the design of offshore wind power plants. For this purpose, a computational fluid dynamics (CFD) approach using large-eddy simulations (LES) was adopted in the present study. An in-house LES-solver based on the actuator line (AL) aerodynamics technique was constructed in order to successfully capture the wake structure behind the wind turbine. First, experimental investigations on both a blade-only wind turbine scale model and a full 3D wind turbine scale model (isolated wind turbine) were conducted for a fixed inlet wind condition, the latter including the nacelle and the tower. Through a detailed comparison of the wind tunnel experimental and numerical results, the prediction accuracy of the in-house LES-solver was verified and validated for fixed inlet wind conditions. On the basis of the validation results obtained, and using the full 3D wind turbine scale model, the effects of the continuously changing inlet wind conditions on the wake characteristics in the near- and far-wake regions were numerically investigated. In addition, the effects of the wind turbine nacelle and tower on the wake characteristics were also investigated. The numerical results show that the most significant impact of the effects of the continuously changing wind direction was the rapid recovery of the mean velocity deficits in the wind turbine wake region. Further, at the x = 10D position (D is the rotor diameter) downstream of the wind turbine, the non-dimensional streamwise mean velocity was 0.93, which nearly matches the approaching flow speed, under an optimal tip speed ratio of 4.0, compared to the fixed wind direction scenario.

## 1. Introduction

In October 2020, the Japanese government declared its intent to reduce greenhouse gas emissions to net zero by 2050, setting Japan on course to become a carbon-neutral society. Based on this, in December 2020, the Ministry of Economy, Trade and Industry took the lead in formulating the Green Growth Strategy for carbon neutrality by 2050, in collaboration with relevant ministries and agencies (Ministry of Economy, Trade and Industry, 2020). The Green Growth Strategy is the key to helping Japan achieve this ambitious goal. In the Green Growth Strategy, 14 priority areas have been set out, as well as numerical targets and countermeasures for certain issues. In particular, offshore wind power generation is expected to play a major role in meeting future energy needs while mitigating climate change and environmental pollution.

Offshore wind facility design and engineering depends on site-specific conditions such as water depth, seabed geology, wave loading, incoming atmospheric boundary layer (ABL) turbulent flow, and wind turbine wake. This paper focuses on understanding wind turbine wakes, with an emphasis on the effect of an oscillation inlet wind velocity on wind turbines on flat terrain, which includes offshore wind turbines.

Similarly to the work of Sedaghatizadeh et al. (2018), Fig. 1 shows a schematic diagram of the aerodynamics of wind turbine wakes on flat terrain and over bodies of water. With the rotation of the blades of the wind turbine, a region of wind velocity deficit, with temporal and spatial

* Corresponding author.
*E-mail addresses:* takanori@riam.kyushu-u.ac.jp (T. Uchida), yves.gagnon@umoncton.ca (Y. Gagnon).

https://doi.org/10.1016/j.jweia.2021.104869
Received 20 May 2021; Received in revised form 30 November 2021; Accepted 1 December 2021
Available online 16 December 2021

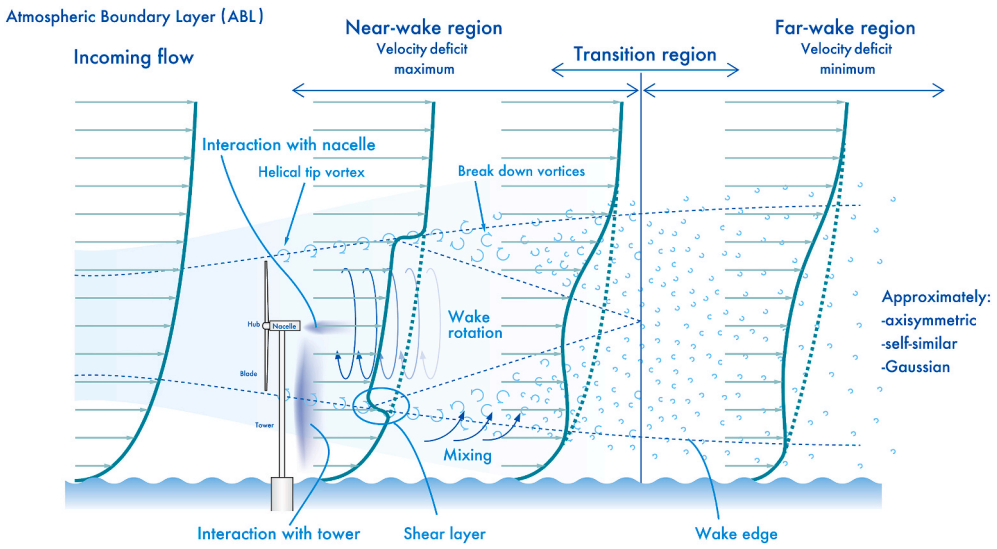


**Fig. 1.** Schematic side view of the wake structure behind single wind turbine.

variations, is formed downstream of the wind turbine. This wind turbine wake can be separated in two zones. The near-wake region is characterized by the maximum velocity deficit and strong shear at the exterior limits of the wake, while the far-wake region is characterized by the minimum velocity deficit and a Gaussian shaped shear of the velocity distribution in the wake.

In application to wind energy, understanding the effects of the ABL turbulence on wind-turbine wake flows is of interest. Indeed, since onshore and offshore wind power plants are designed to have clusters of wind turbines, wake flows have impacts of the overall efficiency of the wind power plant. Not only does wake flows induce considerable turbine power losses due to the wind velocity deficit, the wind turbines are subject to increased fatigue loading due to the added turbulence intensity generated by the upstream turbines. From a fluid mechanics perspective, Hewitt et al. (2018) and Porté-Agel et al. (2020) summarized recent experimental, computational and theoretical research efforts that have contributed to improving our understanding and ability to predict the interactions of ABL turbulent flows with wind turbines and wind power plants.

The mutual interference of wind turbine wakes, which is a strongly nonlinear flow phenomenon, occurs especially in large offshore wind farms consisting of multiple wind turbine groups. Therefore, in order to improve the power efficiency and the lifetime of a wind turbine, an accurate understanding of single turbine wake behavior under various flow conditions is necessary. Furthermore, the thermal stability of the ABL is known to play a significant role on wind turbine performance as well, as it affects the structure and dynamics of wind turbine wake flows. Thus, the main effects on standalone turbines are due to the changes in mean shear and turbulence intensity of the incoming flow, associated with changes in thermal stability. Many findings on these topics have already been reported from wind tunnel experiments (Whale et al., 2000; Chamorro et al., 2010; Zhang et al., 2013; Hancock et al., 2014), field observations (Baker et al., 1984; Magnusson et al., 1999; Iungo et al., 2014; Aitken et al., 2014a; Machefaux et al., 2016; Abraham et al., 2019; Uchida et al., 2021), statistical modeling (Braunbehrens and Segakini, 2019), and numerical simulations (Wu et al., 2012; Churchfield et al., 2012; Keck et al., 2014; Aitken et al., 2014b; Mirocha et al., 2015; Abkar et al., 2015; Machefaux et al., 2016; Draper et al., 2018; Sedaghatizadeh et al., 2018; Uchida et al., 2020, 2021; Uchida, 2020). In the above studies, the effects of turbulent mixing on the wake recovery of a wind turbine are mainly discussed.

Specific to the effect of the flow confinement on the wind turbine wake dynamics, Segalini and Inghels (2014) studied the effect of confinement in wind tunnel measurements of wind turbine wakes by means of a simplified numerical model, which shows that the wake structure achieves its asymptotic state more quickly in the confined condition than in the unconfined one. For their part, using Large Edy Simulations, and comparing with WAsP results, Mo et al. (2013) studied the dynamics of wind turbine wakes, which included assessing the effect of a confinement in a wind tunnel experiments. Finally, Sedaghatizadeh et al. (2016) modeled the NREL phase VI wind turbine in two computational domains, i.e., one representing the confined flow of the wind tunnel experimental data on the same type of wind turbine obtained from the scientific literature, and an unconfined computational domain. Their work reveals that the confinement of the flow affects the dynamics of the wake, and that the 10% limit for blockage ratio reported in previously published literature is not sufficient to eliminate the effect of wind tunnel walls. Such results show that particular attention should be given to the confinement effects on the dynamics of the wake downstream of wind turbines when studied in wind tunnel experiments.

Other research work has been done on the wake effects of wind turbines in complex terrain (see for example the experimental work of Tian et al., 2018), while Abdelsalam et al. (2014) have studied wake turbine wake behavior through numerical modeling and in-situ experimental measurements. For their part, Sessarego et al. (2018) presented a comprehensive study on the aerodynamics of wind farms and a specific wind turbine within the wind farm, using experimental in-situ measurements and CFD modeling (using Reynolds-Averaged Navier-Stokes (RANS) and Large Eddy Simulation modeling).

Considering the wake characteristics of a utility-scale wind turbine under realistic atmospheric boundary layer conditions, the wind direction is continuously changing. Therefore, understanding the effects of continuously changing the incoming wind direction upstream of a wind turbine is of interest in predicting and maximizing the power output of a wind turbine. Thus, in application to onshore wind power plants on flat terrain and offshore wind power plants, understanding the wake characteristics of a wind turbine over flat terrain is necessary in the design of wind farm layouts and in the operation of the power plants.

In this regards, Porté-Agel et al. (2013) investigated the effects of changing the incoming wind direction on the turbine wakes and associated power losses in the Horns Rev offshore wind farm by using large-eddy simulations (LES) techniques. In their numerical study, simulations with a series of different fixed incoming wind directions were carried out. However, the effects of continuously changing the inlet wind direction on the wake characteristics were not investigated.

Therefore, the main focus of this paper is to study the effect of

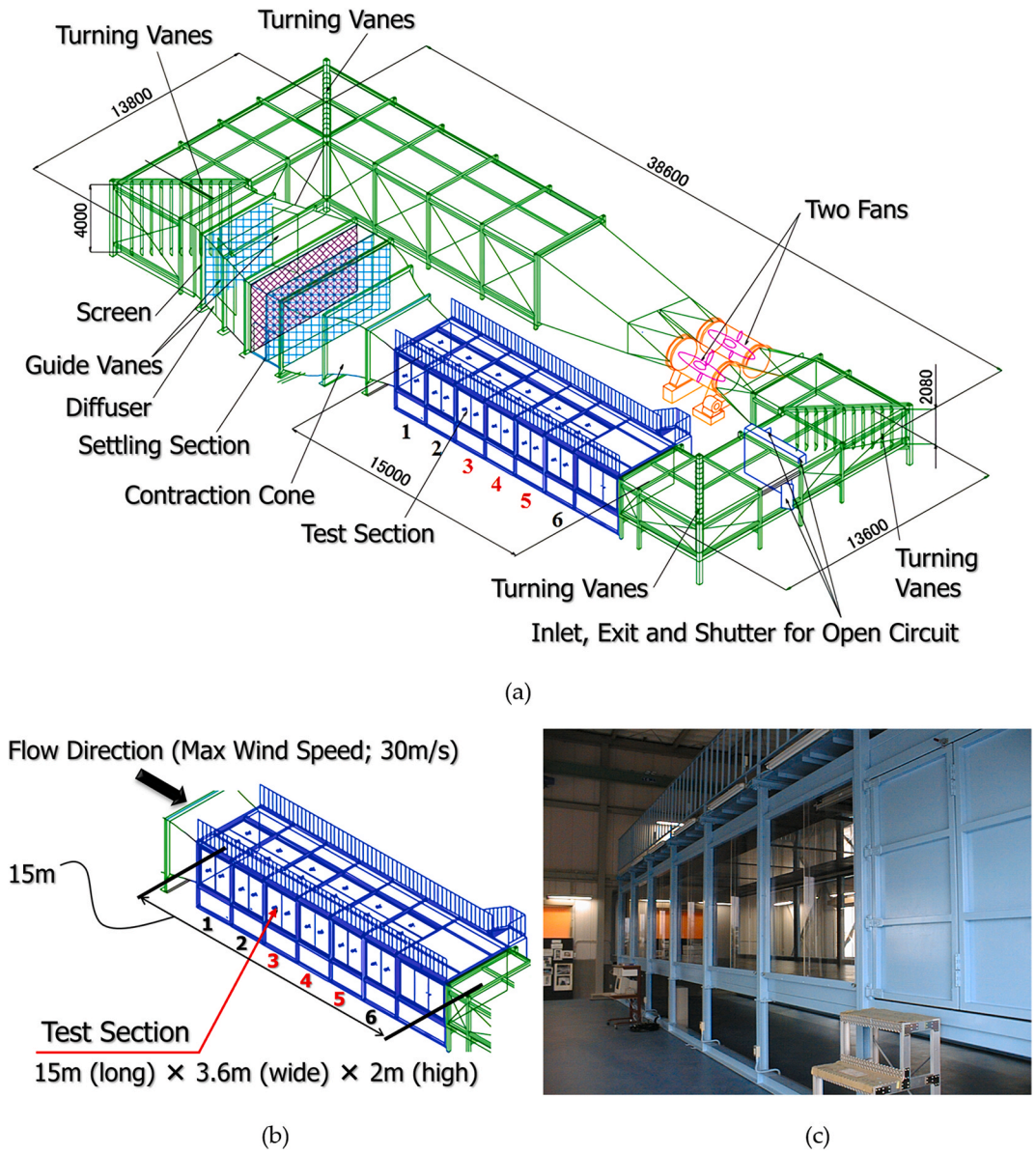


**Fig. 2.** Closed-circuit wind tunnel facility used in this study: (a) perspective view, (b) enlarged view of the test section, (c) photo of the side wall of the wind tunnel.

continuously changing the inlet wind direction on the wake characteristics of a full 3D wind turbine scale model. A computational fluid dynamics (CFD) approach using large-eddy simulations (LES) was employed, with the modeling methodology validated with experimental results. An in-house LES-solver, called RIAM-COMPACT (Uchida et al., 2011a, 2011b; Uchida and Li, 2018; Uchida and Takakuwa, 2019), was developed based on a Cartesian staggered grid and an actuator line (AL) model for the rotation of the wind turbine blades, which is a relatively straight-forward approach for the numerical simulations of multiple wind turbines (Porté-Agel et al., 2020).

First, in order to verify the prediction accuracy of the LES-solver, wind tunnel experiments were performed using a blade-only wind turbine scale model and fixed inlet wind direction, where the numerical and experimental results were compared for tip speed ratios of 2.0, 3.0, 4.0 and 5.0. Next, the flow around a full 3D wind turbine scale model, including the nacelle and the tower, and fixed inlet wind direction was simulated for an optimal tip speed ratio (TSR) of 4.0; these results were also validated with corresponding wind tunnel experimental data.

Wind turbines must be designed with an optimal TSR to get the maximum amount of power from the wind. On the basis of the validation results obtained, and using the full 3D wind turbine scale model operating at the optimal TSR, the effects of continuously changing the inlet wind direction on the wake characteristics in the near- and far-wake regions of the wind turbine were numerically investigated. In addition, the effects of the wind turbine nacelle and tower on the wake characteristics were also investigated in this work.

## 2. Validation of the in-house LES-Solver with a blade-only wind turbine scale model

### 2.1. Wind tunnel experiment using blade-only wind turbine scale model

First, a wind tunnel experiment using a blade-only wind turbine scale model was conducted to verify the prediction accuracy of the in-house LES-solver based on a Cartesian staggered grid.

Wind tunnels are classified in two main types: open-circuit and closed-circuit. In an open-circuit tunnel, the air flow follows a straight path from the entrance through a contraction zone to the test section, and then moves into a diffuser, a fan section, and an outlet. In a closed-circuit wind tunnel, the air recirculates continuously with little or no

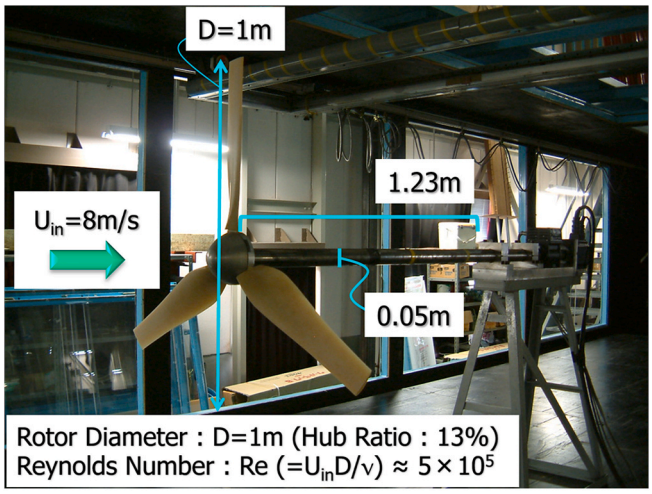


(a)

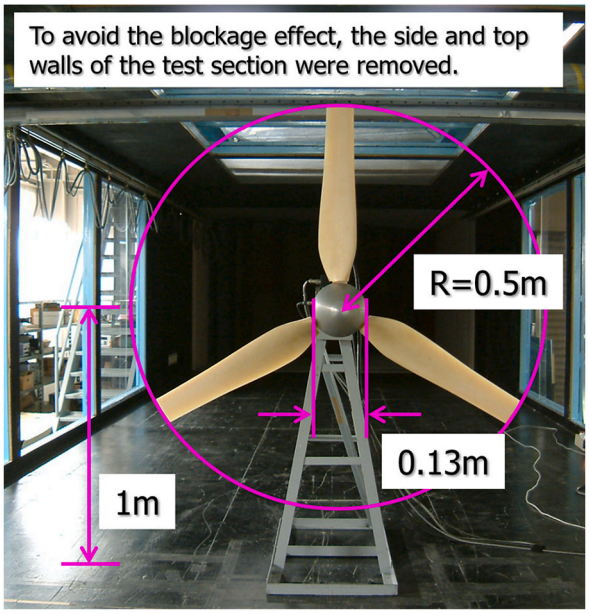


(b)

**Fig. 3.** Blade-only wind turbine scale model used in this study: (a) perspective view, (b) front view.

exchange with the outside. The wind tunnel facility used in this study is a closed-circuit boundary layer wind tunnel (test section: 15 m long × 3.6 m wide × 2.0 m high) of the Research Institute for Applied Mechanics (RIAM) of Kyushu University, as shown in Fig. 2. Fig. 2a presents the overall view of the facility, while Fig. 2b presents an enlarged view of the test section and Fig. 2c shows the side wall of the wind tunnel, looking in the upstream direction. Detailed studies performed with this facility have been published in the literature. Notably, Ohya et al. (2010) studied the concept of shrouded wind turbines generating high output power with the Wind-lens technology, while Göltenbott et al. (2017) presented a detailed description of the facility in their study of the aerodynamic interaction of diffuser augmented wind turbines in multi-rotor systems.

The blade-only wind turbine scale model is shown in Fig. 3, consisting essentially of three blades attached to a common hub, without a nacelle box or a tower. The blades of the small-scale wind turbine model are based on the airfoils designed by Matsumiya et al. (2011). To minimize the blockage effect in the wind tunnel, on the basis of previous work with this facility (notably the work of Ohya and Karasudani (2010) and Göltenbott et al. (2017), the third, fourth and fifth sides and the top walls (shown in red) of the test section (see Fig. 2) were removed. As shown in Fig. 3, the inflow wind velocity ($U_{in}$) was set to 8 m/s in the wind tunnel experiment. The optimal tip speed ratio (TSR = 4.0, about 600 rpm), with the maximum power coefficient (Cp) of the wind turbine scale model, was estimated by rotating the wind turbine blades at multiple rotational speeds. The Reynolds number Re = $U_{in}$ D/$\nu$ determined for a rotor diameter D of 1 m was in the order of $10^5$, where $\nu$ is the kinematic viscosity of the fluid.

In order to assess the confinement effect of the wind tunnel facility, Fig. 4 presents the non-dimensional average velocity in the centerline of the wind tunnel with the blade-only wind turbine scale model and a fixed inlet flow condition, for two cross-sections (x = 5 D and x = 10 D downstream of the nacelle), and for the wind tunnel with and without walls. From this figure, it can be observed that the wind speed distribution in the wind turbine wake is affected by the confinement of the flow, which has been reported in the scientific literature by Sedaghatizadeh et al. (2016). At x = 5 D downstream of the wind turbine, the velocity profiles for the experiment without walls (i.e., when the top and three side panels are removed), underestimate the wake velocities in comparison to the equivalent experiment in a wind tunnel with walls. Furthermore, at x = 10 D, the velocity profile for the experiment without walls overestimates the wake velocities in comparison to the equivalent experiment in a wind tunnel with walls. These differences have also been reported by Sedaghatizadeh et al. (2016).

### *2.2. Overview of the in-house LES-Solver for the blade-only wind turbine scale model*

The simulations of the in-house LES-solver for the blade-only wind turbine scale model (rotor diameter D = 1 m) were performed with various TSR (2.0, 3.0, 4.0, and 5.0), as estimated in the wind tunnel experiment. The in-house LES-solver employs three-dimensional, unsteady, incompressible, filtered-continuity and Navier–Stokes equations with Cartesian co-ordinates. These governing equations are discretized via a finite-difference method (FDM). A mixed timescale (MTS) model (Inagaki et al., 2005) was used for the subgrid-scale (SGS) LES. A major feature of this model is that it does not require a van Driest-type wall-damping function to reduce the effects of the model's viscosity near the walls, and it is easily applied to complex turbulent flows.

For the rotation of the wind turbine blades, an actuator line (AL) model was used to approximate the individual rotor blades as lines of body force, without resolving all of the geometrical details and the boundary layer resolution of the wind turbine. In the AL model, the tangential and thrust forces generated by the rotating blade are added to the filtered Navier–Stokes equations as external force terms that represent the reaction forces exerted on the fluid in the direction of streamwise flow and rotation. The AL model applies body forces to the flow along rotating lines which model the individual blades, thus giving the fluid resistance as the wind turbine blades rotate. The appeal of the model is for the simple mesh needed, and the low computational costs. Therefore, the AL model is not capable of predicting partial or local separation on the blades.

In the present study, because a Cartesian grid system is adopted, the force in the direction of rotation has been decomposed into the spanwise and vertical directions. This method gives a realistic approximation of the turbine wake's structure with only the blade chord length, the lift coefficient, the drag coefficient, and the angle of attack (as a function of the distance from the center of the rotor) as inputs. Furthermore, the AL method has significantly increased the computational speed compared to the blade-resolved CFD simulation with the use of the sliding mesh technique. The LES simulations in the present study were performed using a new SX-Aurora TSUBASA vector supercomputer. The CPU time required for each calculation was several days. In previous work, the in-house LES-solver and the RANS-based commercial CFD software have

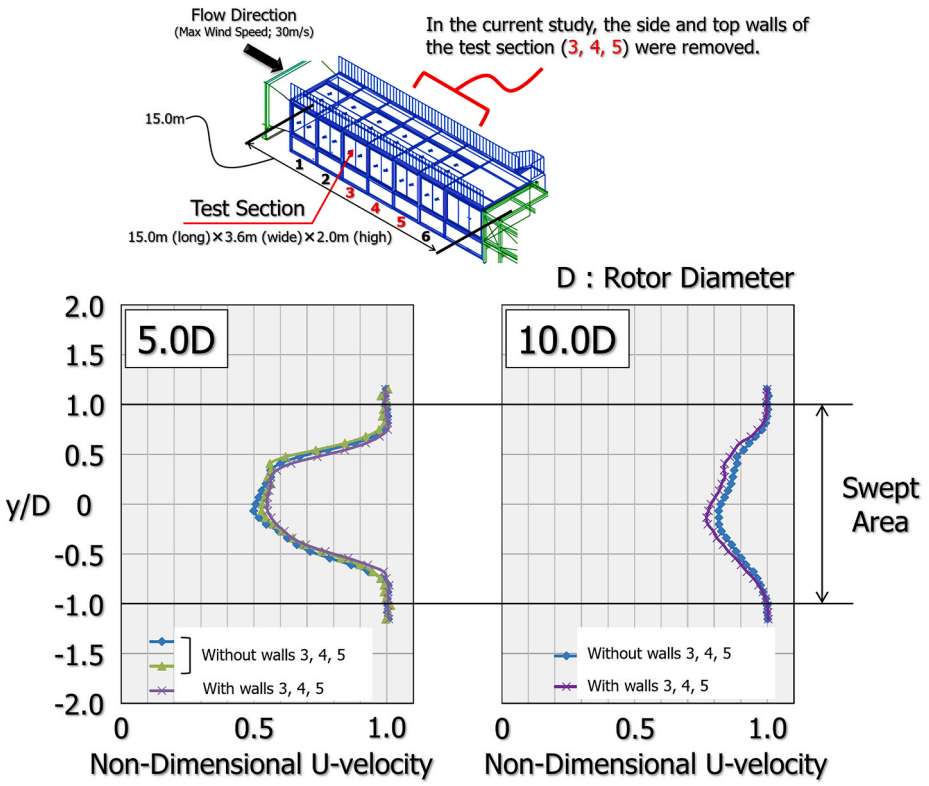


**Fig. 4.** Non-dimensional average velocity in the centerline of the wind tunnel, for two cross-sections (x = 5.0D and x = 10.0D downstream of the nacelle), and for the wind tunnel with and without walls.

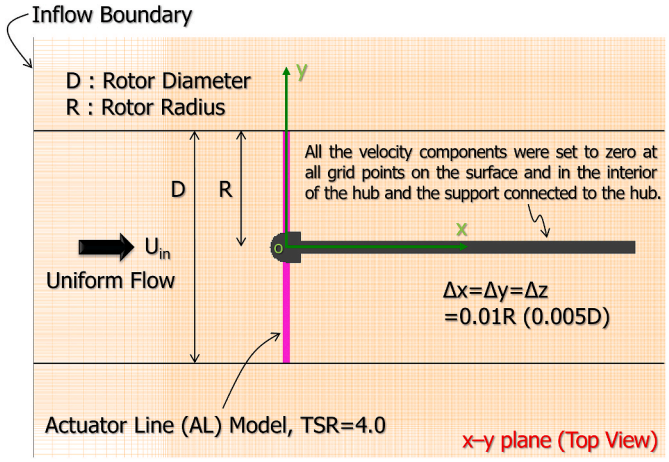


**Fig. 5.** Enlarged view of the computational grid in the numerical simulation of the wind tunnel experiment using a blade-only wind turbine scale model: x–y plane (top view).

been compared, and it has been shown that the in-house LES-solver provides comparable results as the RANS-based commercial software (Uchida and Li, 2018).

Wind turbine wake flows are characterized by complex 3D phenomena and turbulent structures that impose fine grid resolutions, not only in the streamwise direction, but also in the other two directions. Fig. 5 shows an enlarged view of the computational grid used in the numerical simulation for the wind tunnel experiment using a blade-only wind turbine scale model. The total number of grid points in the computational domain was approximately 235 million [2021 (x) × 341 (y) × 341 (z)]. The uniform spatial resolution in the three directions behind the wind turbine model (Δx, Δy, and Δz) was 0.01R, where R is the radius of the rotor of the wind turbine model. As explained earlier, in order to model the rotation of the turbine blades, the AL method (based on blade-element theory) is applied. All the velocity components are set to zero at all grid points on the surface and in the interior of the hub, and in the support connected to the hub. Here, the motor was not simulated in order to focus only on the flow through the blades. The lateral, upper and lower boundary conditions were assigned a slip condition, while the outflow section was assigned a convection-type outflow condition. The time step is $\Delta t = 5 \times 10^{-4}$ ($R/U_{in}$). To fully develop the flow field in both near- and far-wake regions downstream of the wind turbine model, time integration from t = 0 to 65 ($R/U_{in}$) were performed.

### 2.3. Validation of the in-house LES-Solver with a blade-only wind turbine scale model

First, the airflow structure of the wind turbine's wake at the optimal TSR (4.0) was assessed. Fig. 6 shows the spatial distribution of the non-dimensional vorticity for a typical, instantaneous flow field. Focusing on the top view (Fig. 6a), the periodic formation of a tip vortex is clearly observed near the tip of the wind turbine blade, up until x = 4D in the near-wake region. Afterwards, the tip vortex gradually collapses in the far-wake region, beyond x = 4D, due to aerodynamic instabilities. As a result, both the meandering motion and the subsequent turbulent mixing were confirmed in the turbine wake flows.

The rear views in Fig. 6b–e shows the concentric wake flows that are formed with the formation of the tip vortex, notably at x = 2D and 4D in the near-wake region. However, in the far-wake region, beyond x = 4D, the concentric wake flows are significantly deformed due to the collapse of the tip vortex. In addition, turbulent mixing is promoted due to the instabilities in the tip vortex.

The time-series data of the wind speed at the position immediately downstream of the wind turbine blade at the optimal TSR (4.0) were acquired in both the wind tunnel experiment and the numerical simulation. Based on these time-series data, the blade passing frequency

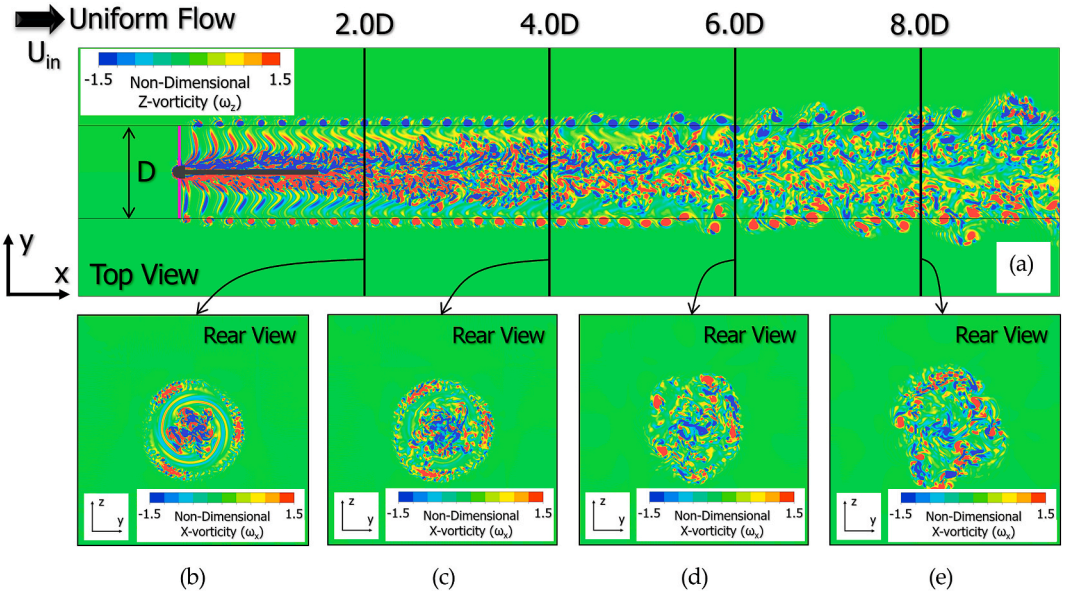


**Fig. 6.** Spatial distribution of the non-dimensional vorticity in a typical, instantaneous flow field: (a) x–y plane (top view), (b–e) y–z plane (rear view); (b) x = 2D, (c) x = 4D, (d) x = 6D, and (e) x = 8D.

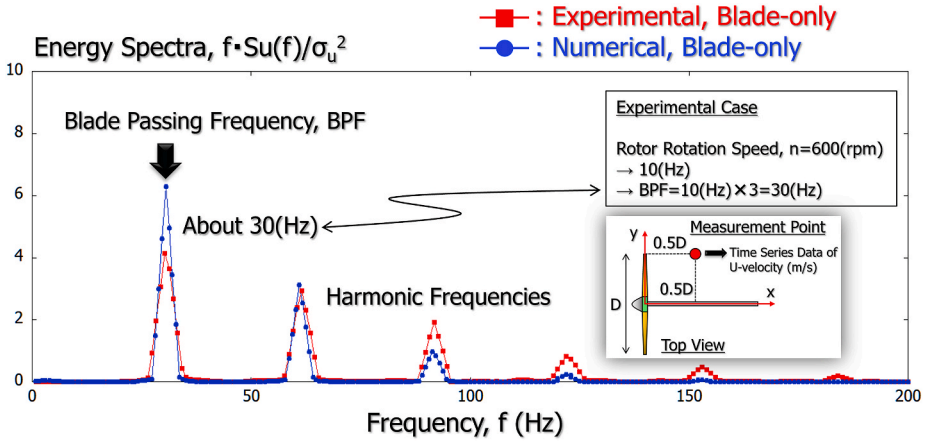


**Fig. 7.** Comparison of the blade passing frequency (BPF) values measured in the blade-only wind tunnel experiment and computed in the numerical simulation.

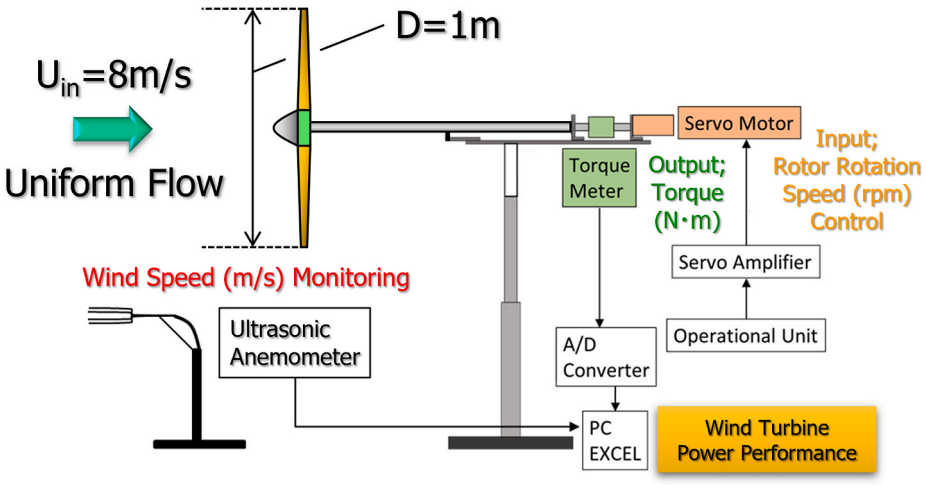


**Fig. 8.** Schematic view of the torque-measurement system used in the performance test.

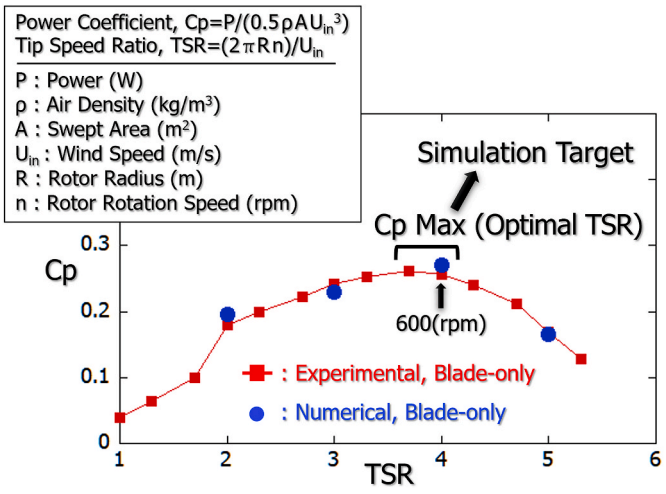


**Fig. 9.** Relationship between the time-averaged tip speed ratio (TSR) and the power coefficient (Cp) of the blade-only wind turbine scale model.

(BPF) values were evaluated and compared.

The time-series data of the experimental wind speed in the streamwise direction (U-velocity) were acquired by a conventional bridge-feedback amplifier constant-temperature hot-wire anemometer system, while a single hot-wire anemometer probe (0251R-T5, Kanomax, Japan), containing a 5 μm tungsten wire with a sensitive length of about 2 mm, was used to determine the wind speed. The sampling rate was set at 500 Hz, and the sampling time was set at 30 s in order to investigate the mean flow characteristics of the flow. As such, the time series data comprised 15,000 data groups.

Fig. 7 shows a comparison of the blade passing frequency (BPF) values measured in the blade-only wind tunnel experiment and computed in the numerical simulation. In this figure, the appearance of the blade passing frequency (BPF) and its multiple frequencies are clearly confirmed. Further, this figure shows that there is a good agreement, qualitatively and quantitatively, between the experimental and numerical results. Thus, these results validate that the numerical model can accurately simulate the behavior of the periodic release of the tip vortex measured in the wind tunnel experiment.

Finally, the power coefficients (Cp) for a variety of TSR (2.0, 3.0, 4.0, and 5.0) were evaluated through the wind tunnel experiment and the numerical simulations, and the results obtained were compared. Fig. 8 shows a schematic view of the torque-measurement system used in the performance test. Fig. 9 shows the relationship between the time-averaged TSR and Cp of the blade-only wind turbine scale model, as measured in the wind tunnel experiment. The same indicator computed in the numerical simulations is overlayed on this figure. It can be observed that the numerical model almost perfectly reproduces the results of the wind tunnel experiments at all TSR. From the comparison between the wind tunnel experiment and the LES results, it can be determined that the AL method implemented in the in-house LES-solver can accurately reproduce the performance of the blade-only wind turbine scale model.

## 3. Validation of the in-house LES-Solver with a full 3D wind turbine scale model

A full 3D wind turbine scale model, including the nacelle and the tower, was created for more realistic simulations. The prediction accuracy of the in-house LES-solver was further validated using this wind turbine scale model.

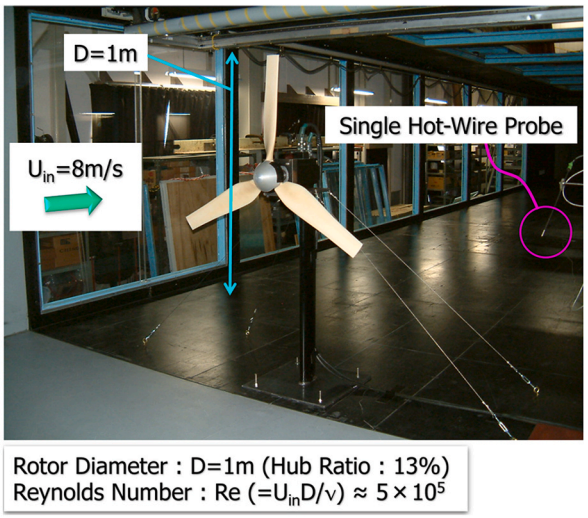


(a)

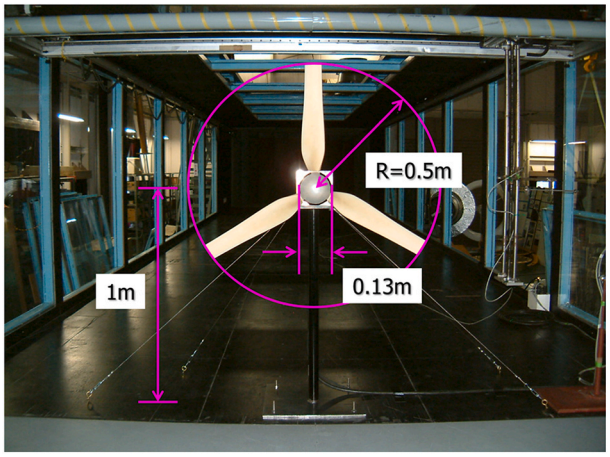


(b)

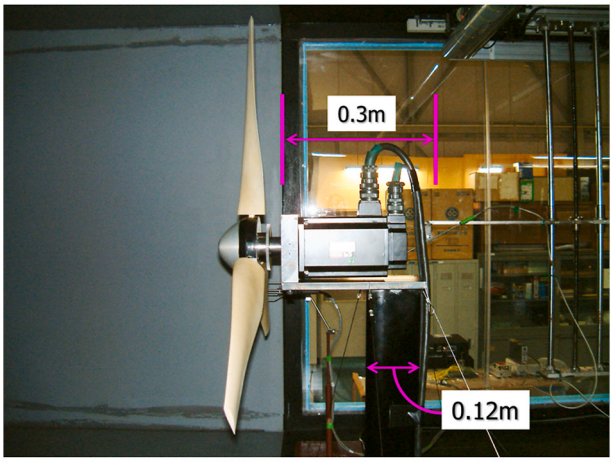


(c)

**Fig. 10.** Full 3D wind turbine scale model used in this study: (a) perspective view, (b) front view, (c) side view.

### 3.1. Wind tunnel experiment using a full 3D wind turbine scale model

Fig. 10 shows the full 3D wind turbine scale model used in the experimental investigation. Here, the 1 m diameter blade is the same as that shown in Fig. 3. The wind turbine scale model was installed at the

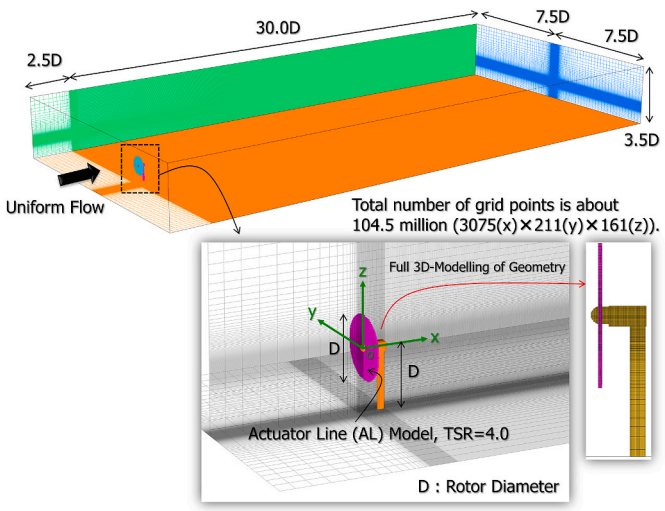


**Fig. 11.** Computational domain and grid used in the numerical simulation for the wind tunnel experiment using the full 3D wind turbine scale model.

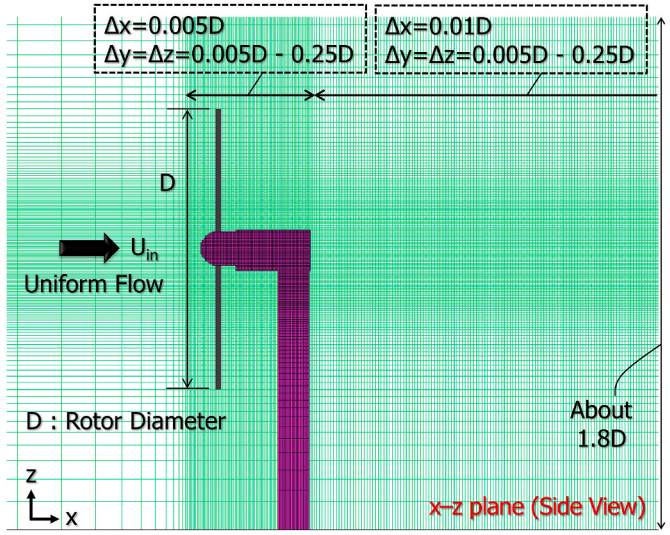


**Fig. 12.** Enlarged view of the computational grid in the x–z plane (side view) for the full 3D wind turbine scale model.

most upstream part of the test section, shown in Fig. 2, in order to investigate the characteristics of the mean velocity in the far-wake region using a single hot-wire probe. The probe was attached to the three-dimensional fully automated traverse (coordinated) system; and could be moved to any position via computer control. In this part of the study, the wind tunnel experiment was conducted by focusing on the optimal tip speed ratio designed to derive the maximum power from the wind. The other experimental conditions were the same as for the blade-only wind turbine scale model.

### 3.2. Overview of the in-house LES-Solver for the full 3D wind turbine scale model

The wake structure for the full 3D wind turbine scale model was studied with the in-house LES-solver at the optimal TSR (4.0), which was identified in Fig. 9. Fig. 11 shows the computational domain and the grid distribution, where the total number of grid points in the computational domain was about 104.5 million [3075 (x) × 211 (y) × 161 (z)]. In order to examine the detailed behavior of the flow in the far-wake region, a computational domain of sufficient length, extending 30D downstream of the model, was established on the downstream side of the wind turbine scale model. In addition, a sufficiently wide region in the spanwise direction was established, corresponding to a total width of 15D. The spatial resolutions in the three directions behind the wind turbine model were sufficiently fine to assure grid independent results, as shown in Fig. 11. Finally, a uniform flow in the horizontal direction (x-y plane) was set for the inflow conditions, which corresponds to the inlet condition of the wind tunnel experiment.

Fig. 12 shows an enlarged view of the computational grid in the x–z plane (side view). To reproduce the conditions of the wind tunnel experiments in the numerical simulations, the configurations of the hub, nacelle and tower were reconstructed with rectangular-grid approximations. This means that all the velocity components were set to zero at all grid points on the surface and in the interior of the hub, nacelle and tower. Further, Fig. 12 presents an enlarged view of the computational grid in the x-z plane. Fig. 12 also confirms the high density of grid points in the vicinity of the blades, the nacelle and the tower, in conformity with analyses published in the literature (Santoni et al., 2017; Abraham et al., 2019; Foti et al., 2019).

### 3.3. Validation of the in-house LES-Solver with a full 3D wind turbine scale model

A top view (x-y plane) of the spatial distribution of the non-dimensional vorticity in the instantaneous flow field is shown in Fig. 13 for the blade-only model (a) and the full 3D model with nacelle and tower (b). Their corresponding side views (x-z plane) are shown in Fig. 14. These figures show the dynamics of the wake and the inherent periodic structures convected downstream. Through careful examination of both Figs. 13 and 14, in the near-wake region of about 5D downstream of the wind turbine scale model, the influence of the nacelle and the tower on the flow field is visible. Fig. 15 presents the non-dimensional vorticity field in the vicinity (up to 5D) of the blade-only model (a) and the full 3D model. The wake characteristics and structures are clearly different, up to at least 5D downstream of the model.

However, Figs. 13 and 14 show that, in the far-wake region 5D or more from the wind turbine, almost no significant difference can be perceived resulting from the presence or absence of the nacelle and the tower. This may be due to the three-dimensional tip vortex distorting and breaking down, leading to increased turbulent mixing. In other words, the effects of the nacelle and the tower on the wake characteristics are limited to the near-wake region, within a 5D region downstream of the wind turbine scale model.

With or without the nacelle and the tower, the wake-meandering phenomenon, which causes the wake to move both horizontally and vertically as it is convected downstream, arises in the far-wake region 5D downstream from the wind turbine. This oscillatory motion of the wake is said to be extremely important in regard to the loading on downstream turbines, notably because it increases the fatigue loads and, more significantly, the yaw loads.

Fig. 16 illustrates the time-averaged non-dimensional U-velocity distribution at the center of the wind turbine hub for the experimental and numerical results used in the validation of the in-house LES-solver. In this figure, the experimental data correspond to the case for the full 3D model with nacelle and tower, while the numerical results are presented for both the blade-only and the full 3D model with nacelle and tower.

After approximately 2D downstream of the wind turbine, the experimental and numerical results for the full 3D wind turbine scale model show good comparisons. In both the wind tunnel experiment and the numerical simulation for the full 3D model, there was a velocity deficit of about 30% with respect to the incoming flow, even at x = 10D. In the vicinity of the wind turbine model (no experimental measurements), the results show the difference in the dynamics of the wake between the full 3D model and the blade-only model. Notably, the full 3D model clearly shows the recirculating flow behind the nacelle and

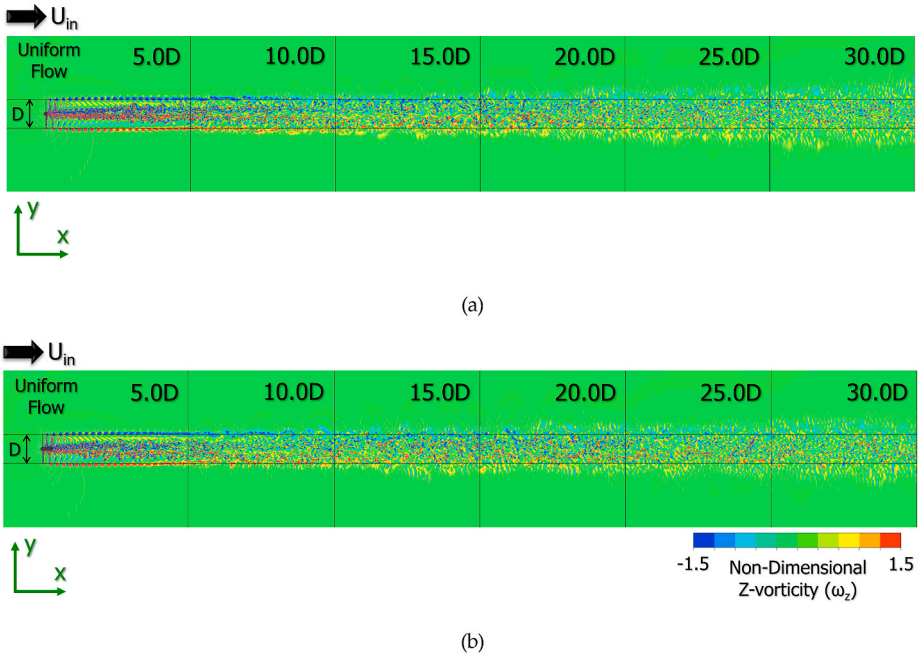


**Fig. 13.** Top view of the spatial distribution of the non-dimensional vorticity in instantaneous flow fields: (a) blade-only model; (b) full 3D model with nacelle and tower.

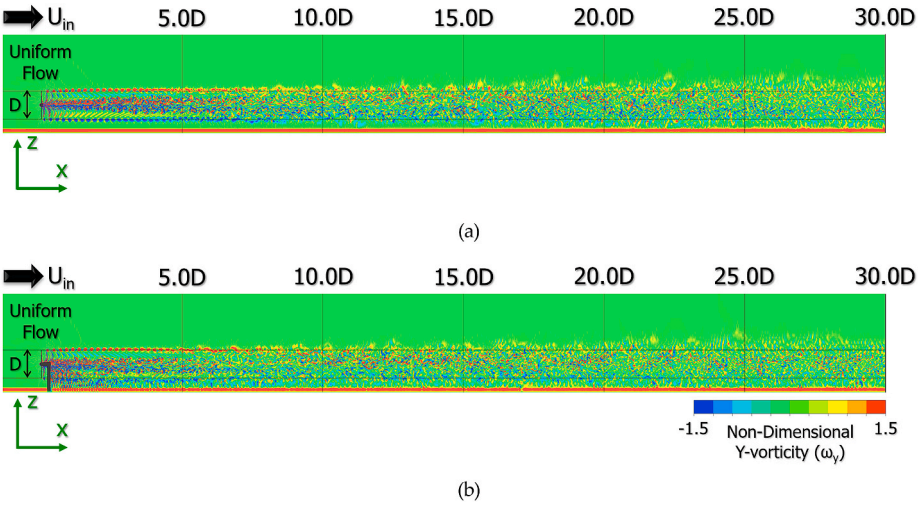


**Fig. 14.** Side view of the spatial distribution of the non-dimensional vorticity in the instantaneous flow field: (a) blade-only model; (b) full 3D model with nacelle and tower.

tower (as indicated by the negative velocities), while the effect of the nacelle and the tower extend to approximately 5D downstream of the model.

In regards to the blade-only numerical results, Fig. 16 shows that the presence of the nacelle and tower has a significant effect on the averaged wind velocity distribution in the near-wake region within 5D downstream of the wind turbine scale model. In the far-wake region further than 5D downstream of the wind turbine scale model, there is a slight but constant difference between the two simulations. The simulation results for the full 3D wind turbine scale model show a more significant wake recovery at greater distances compared to the simulation results for the blades-only model. The nacelle–wake separation is expected to increase turbulent mixing and thus benefit wake recovery.

Fig. 17 shows the non-dimensional U-velocity distribution of horizontal cross-sections in the wake region, together with the wind tunnel experiment results, while Fig. 18 shows the corresponding non-dimensional U-velocity distribution of vertical cross-sections at the same locations.

The results presented on Fig. 17a (X = 5D) and 17b (X = 10D) show good agreements between the numerical and experimental results, notably in the swept area. In particular, the mean velocity profile in the near-wake region (x = 5D) has three clear peaks. Even at x = 10D, in the far-wake region, there is good agreement between the results of both the wind tunnel experiment and the numerical simulations, as shown in Fig. 17b. The turbulence mixing accelerates the wake recovery in terms of both the velocity deficit and the turbulence intensity. In the far-wake region, the velocity deficit resembles a Gaussian profile, which is axisymmetric and self-similar. Furthermore, the meandering motion of the wake might also contribute to the recovery of the velocity deficit, although it significantly increases the unsteadiness of the loading on the downstream turbines.

Fig. 18, on the non-dimensional U-velocity distribution of vertical

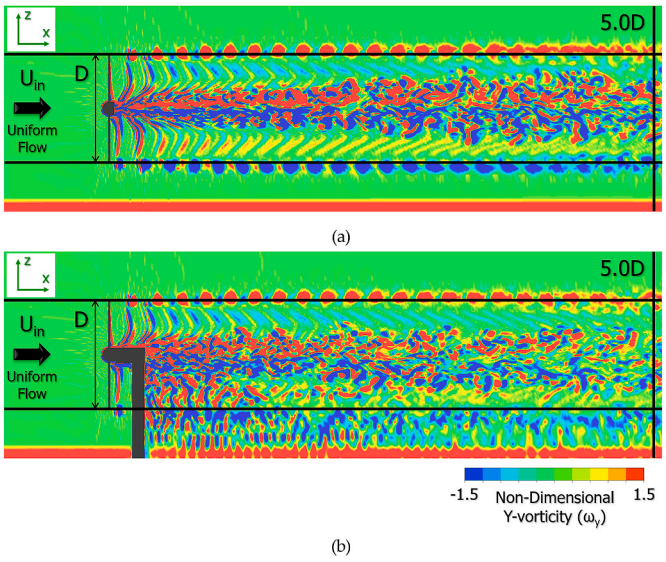


**Fig. 15.** Enlargement of the side view of the spatial distribution of the non-dimensional vorticity in the instantaneous flow field, up to 5D: (a) blade-only model; (b) full 3D model with nacelle and tower.

cross-sections (x–z plane), shows similar behavior of the wake flow in the swept area, and above, for both the blade-only and the full 3D model. Below the swept area, there are significant differences on the flow depending on the presence or absence of the nacelle and the tower. These observations are valid for the two cross-sections presented, at x = 5D and x = 10D.

These numerical results, compared to experimental results, further confirm the validity of the in-house LES-solver to accurately simulate the wake flow of a full 3D wind turbine scale model.

## 4. Continuously changing wind direction on the full 3D wind turbine scale model

The results presented in the previous sections confirm the validity of the in-house LES-solver to simulate the wake flow behind a full 3D wind turbine scale model. In these previous sections, the inlet velocity condition for the numerical models was the same as the experimental wind tunnel model, namely a fixed, uniform velocity condition. Using the same numerical model and the same full 3D wind turbine scale model, the wake characteristics are simulated for an oscillating uniform wind as the inlet condition. This will allow to assess the behavior of the wake when the wind arriving at a wind turbine continuously changes direction, a phenomenon that is often seen in atmospheric boundary layer flows.

### *4.1. Overview of the in-house LES-Solver for the continuously changing wind direction*

Except for the inlet velocity condition, all the other boundary conditions, i.e. for the top, bottom, left-right sides and outlet section, are the same as those explained in section 3.2. Fig. 19 presents a schematic view of the inlet conditions, where the inlet uniform velocity oscillates in the

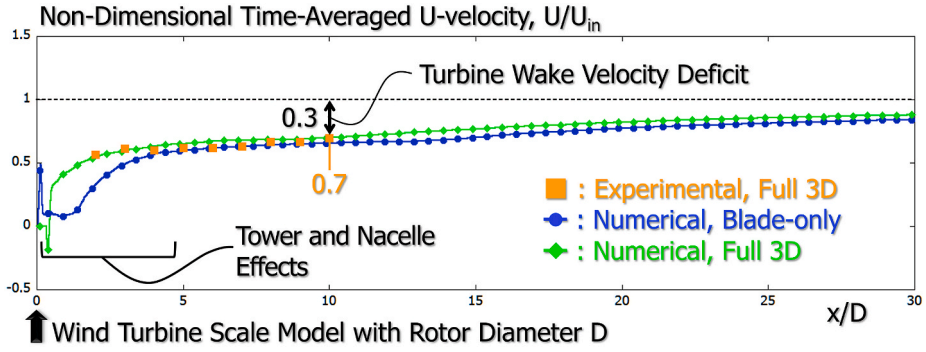


**Fig. 16.** Comparison of the time-averaged non-dimensional U-velocity distribution at the center of the wind turbine hub.

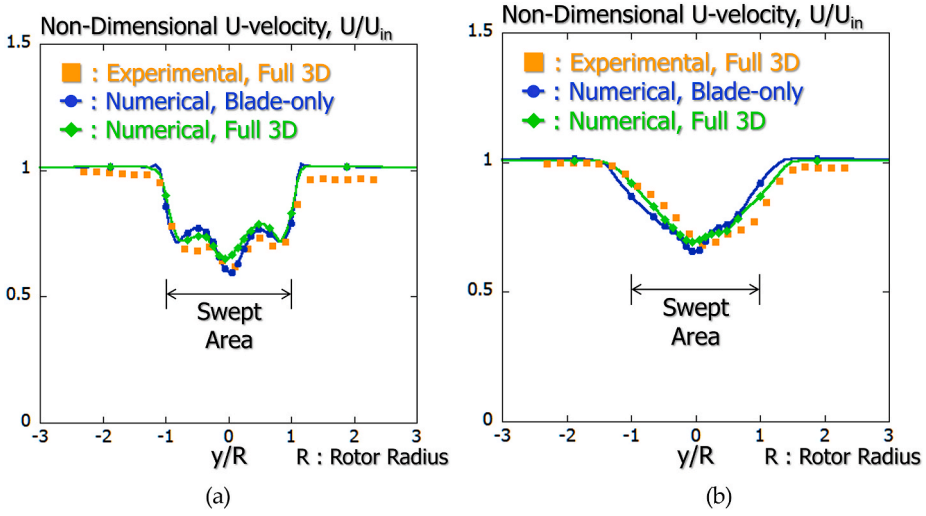


**Fig. 17.** Non-dimensional U-velocity distribution of horizontal cross-sections (x–y plane) in the wake region: (a) x = 5D, (b) x = 10D.

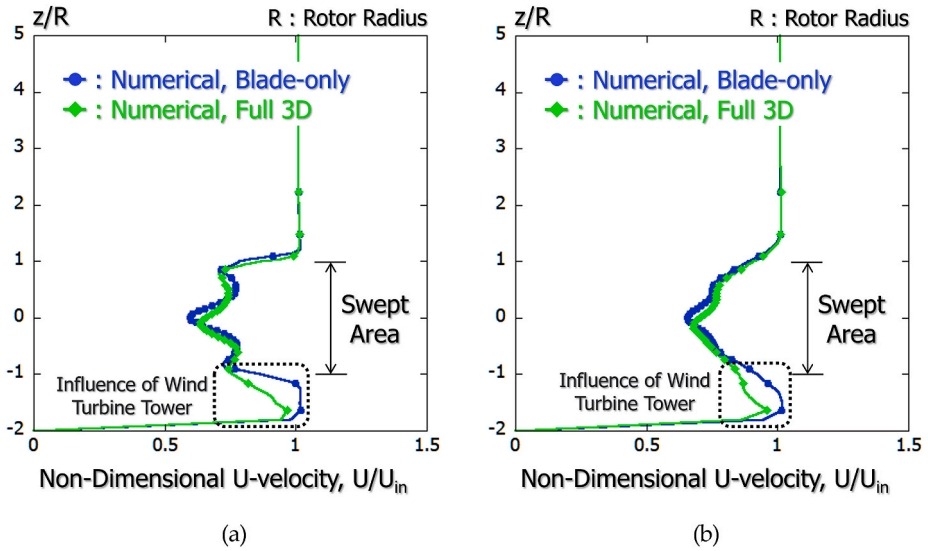


**Fig. 18.** Non-dimensional U-velocity distribution of vertical cross-sections (x–z plane) in the wake region: (a) x = 5D, (b) x = 10D.

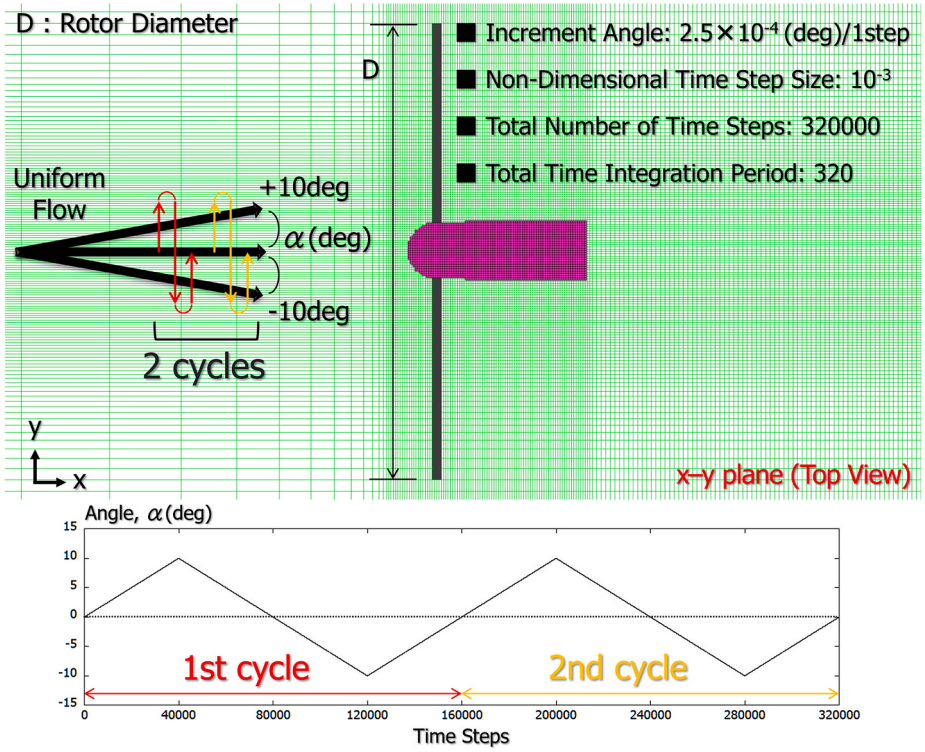


**Fig. 19.** Schematic view of the continuously changing wind direction.

horizontal x-y plane. Since the yaw angle threshold for activating the yaw control system is generally about ±15° in utility-scale wind turbines, a yaw angle of ±10° was set to continuously change in the horizontal (x–y) plane, with a period of 160k time steps. For its part, the velocity in the vertical (z) direction was zero. The increment angle was determined based on the results of our previous similar CFD-sensitivity analysis (Uchida, 2020). Other important simulation parameters are specified in Fig. 19.

### *4.2. Results for the continuously changing wind direction on the full 3D wind turbine scale model*

Fig. 20 shows a top view of the temporal and spatial evolution of the behavior of the wind turbine wake flows visualized as non-dimensional U-velocity in the x–y plane. Fig. 20a (left column) displays a fixed wind direction scenario, while Fig. 20b (right column) displays a continuously changing wind direction scenario. In the fixed wind direction scenario shown in Fig. 20a, in the far-wake region, 5D or more downstream of the wind turbine, three-dimensional tip vortex distortion and breakdown occur, causing the wind turbine wake to meander (meandering flow), as was observed in Figs. 14 and 16. This effect is due to increased turbulent mixing. However, in the continuously changing wind direction scenario shown in Fig. 20b, a dynamic meandering wake phenomenon can be observed due to the oscillation of the wind direction in the horizontal (x–y) plane. In other words, the amplitude of wake meandering increases with the distance downstream from the wind turbine when the

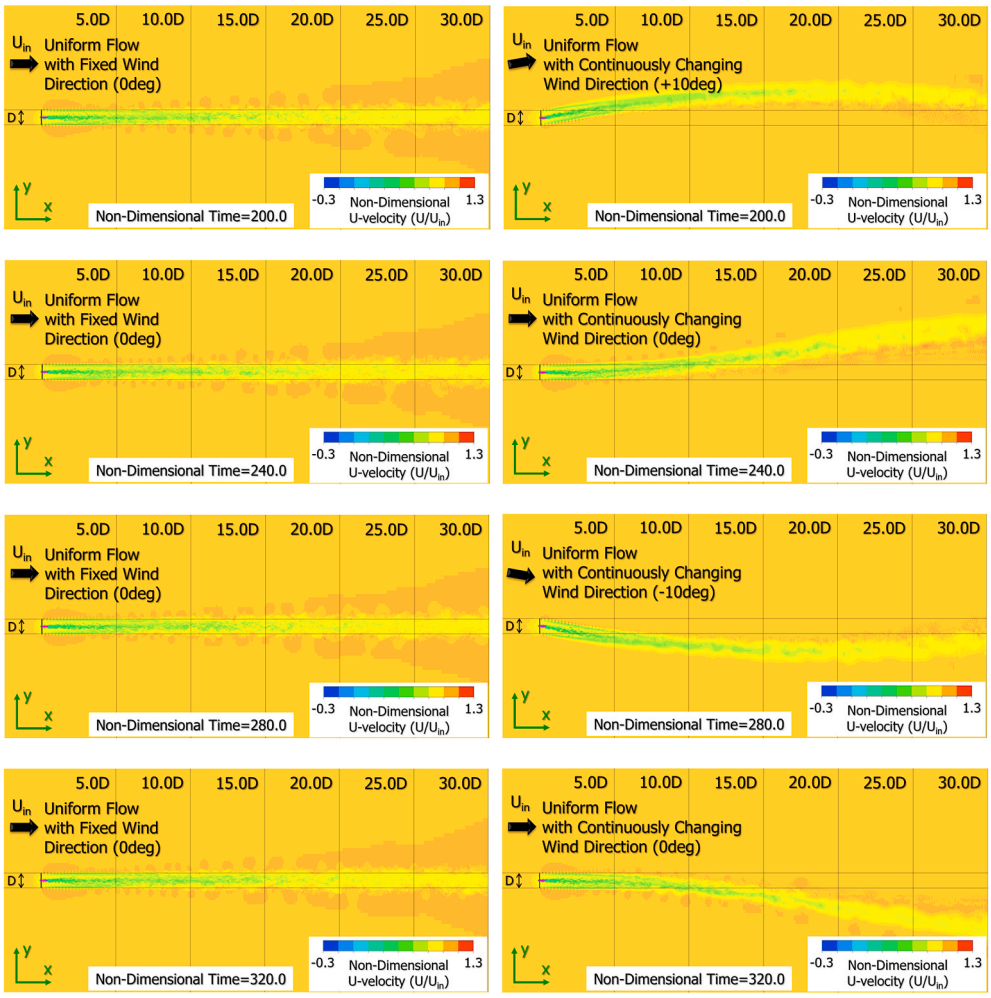


**Fig. 20.** Top view of the temporal and spatial evolution of the wind turbine wake flows visualized via the non-dimensional U-velocity in the x–y plane: (a) fixed inlet wind direction, (b) continuously changing inlet wind direction.

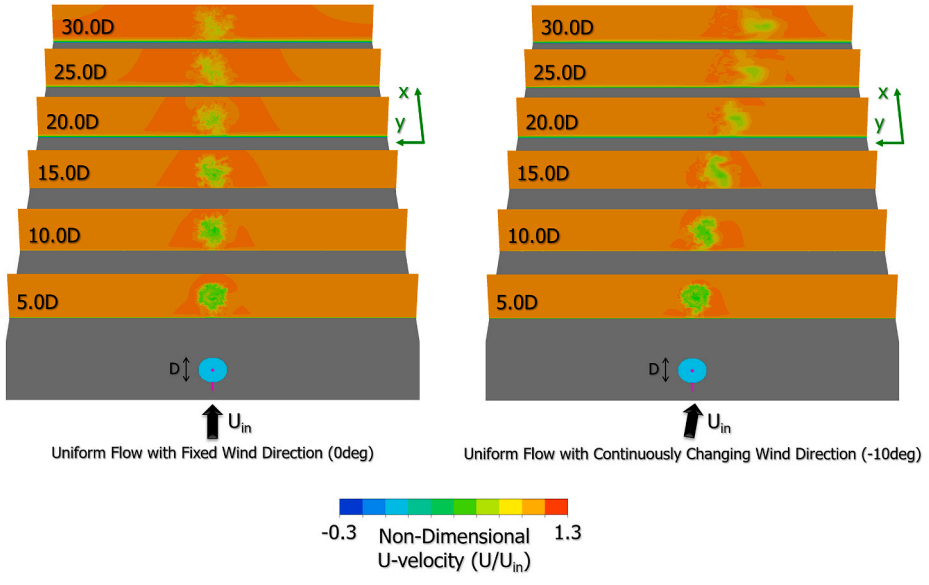


**Fig. 21.** Front view of the spatial distribution of the non-dimensional U-velocity in the y–z plane in the instantaneous flow field (last time: 320): (a) fixed inlet wind direction, (b) continuously changing inlet wind direction.

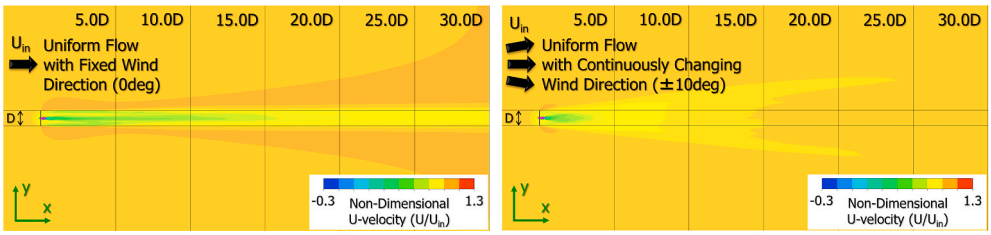


**Fig. 22.** Top view of the spatial distribution of the non-dimensional U-velocity in the x–y plane for the time-averaged flow field: (a) fixed inlet wind direction, (b) continuously changing inlet wind direction.

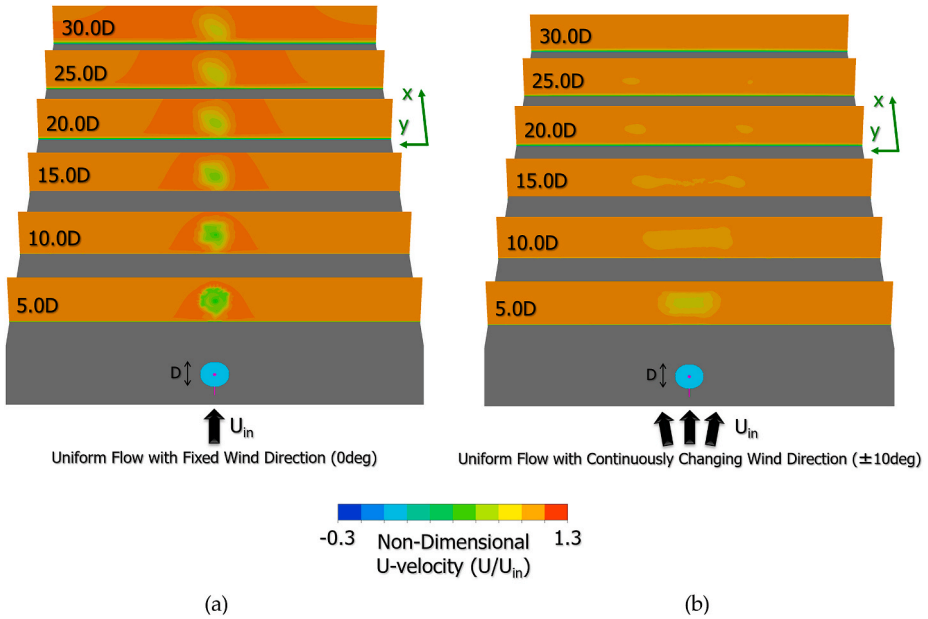


**Fig. 23.** Front view of the spatial distribution of the non-dimensional U-velocity in the y–z plane for the time-averaged flow field: (a) fixed inlet wind direction, (b) continuously changing inlet wind direction.

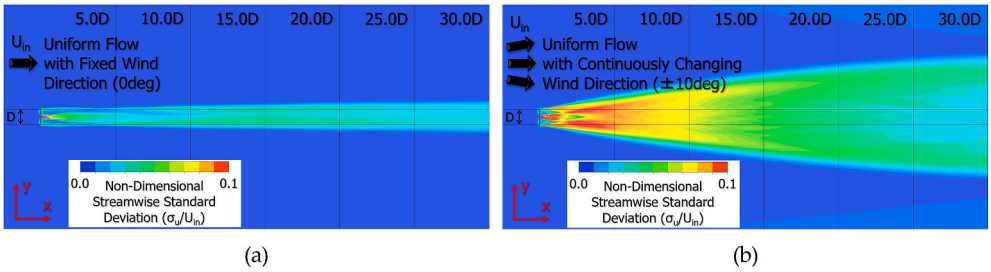


**Fig. 24.** Top view of the spatial distribution of the non-dimensional streamwise standard deviation in the x–y plane for the time-averaged flow field (last time): (a) fixed inlet wind direction, (b) continuously changing inlet wind direction.

inlet flow oscillates in the horizontal plane. Further, from Fig. 20, and confirmed by looking at numerical animations of the flow, the variation in the angle of the incoming flow is highly correlated with the variation in the near wake behind the wind turbine. On the other hand, in the far wake region, there is a significant phase difference between the variation in the wake direction and the angle of the incoming flow.

Fig. 21 shows a front view of the spatial distribution of the non-dimensional U-velocity in the y–z plane for the instantaneous flow field. The non-dimensional time shown here is 320, which is the final point of the time integration. Compared with the fixed wind direction case shown in Fig. 21a, the wake center has shifted significantly from the center line in the scenario of the continuously changing inlet wind direction shown in Fig. 21b. This phenomenon is referred to as wake deflection.

Fig. 22 shows the top view of the spatial distribution of the non-dimensional U-velocity in the x–y plane for the time-averaged flow field, while Fig. 23 shows the corresponding front view of the spatial distribution of the non-dimensional U-velocity in the y–z plane. By carefully considering the simulation results from the fixed inlet wind direction scenario, it can be observed that the spreading rate of the wake shows little change, even at x = 30D, which is sufficiently far from the wind turbine. Furthermore, the wake recovery rate was also extremely small. However, interestingly, the simulation results for the continuously changing inlet wind direction scenario show both a wider

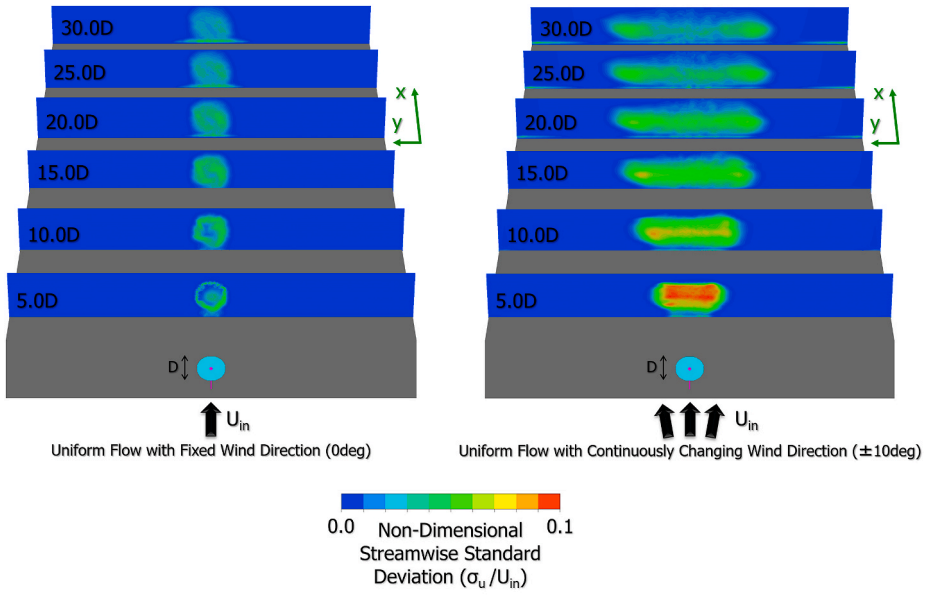


**Fig. 25.** Front view of the spatial distribution of the non-dimensional streamwise standard deviation in the y–z plane for the time-averaged flow field: (a) fixed inlet wind direction, (b) continuously changing inlet wind direction.

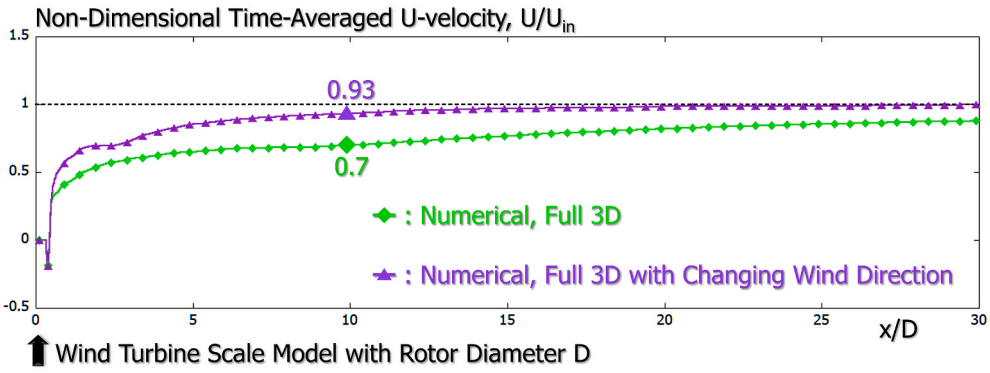


**Fig. 26.** Comparison of the time-average non-dimensional U-velocity distribution at the center of the wind turbine hub.

spreading of the wake and a faster wind speed recovery of the wake flow.

The turbulence characteristics of wind turbine wakes for the scenario of a continuously changing inlet wind direction is now considered. Fig. 24 shows a top view of the spatial distribution of the non-dimensional streamwise standard deviation in the x–y plane for the time-averaged flow field, while Fig. 25 shows the corresponding front view in the y–z plane. Compared with the simulation results for the fixed inlet wind direction scenario, an enhanced turbulence level is clearly observed for the continuously changing inlet wind direction scenario, both in the near- and far-wake regions downstream of the full 3D wind turbine scale model. It can also be seen that the spatial area of the wake expands significantly in the downstream direction. Furthermore, an extremely high turbulence level occurs within x = 10D. This is thought to be caused by the periodic shedding of the tip vortex, which induces turbulent mixing.

Fig. 26 shows a comparison of the time-averaged non-dimensional U-velocity distribution at the center of the wind turbine hub. For the continuously changing inlet wind direction scenario, the mean velocity is recovered more rapidly compared to the fixed inlet wind direction scenario. At the x = 10D position, the non-dimensional streamwise mean velocity is 0.93 in the continuously changing inlet wind direction scenario, which almost reaches the value of the approaching flow; for the fixed inlet wind direction, this velocity is only 0.7 (as confirmed by the experimental results presented on Fig. 16). While we do not have experimental results to confirm the velocity deficit at x = 10D for this flow configuration, we believe that, on the basis of other results validated in this paper, the results are representative of the velocity field at this cross-section. Notably, these results show that the most significant effect of a changing inlet wind direction is the rapid recovery of velocity deficits in the wind turbine wake region.

Fig. 27 compares the non-dimensional standard deviation distribution of the velocity, normalized by the average inlet wind velocity and computed over the second cycle (see Fig. 19), at the center of the wind turbine hub in three directions. In the streamwise standard deviation distribution shown in Fig. 27a, the values for the continuously changing inlet wind direction scenario are clearly larger (up to x = 20D) than in the fixed inlet wind direction scenario. In the far-wake region, which is further downstream, the numerical values in the continuously changing inlet wind direction scenario rapidly approaches the numerical values for the fixed inlet wind direction scenario. In the spanwise direction shown on Fig. 27b, the numerical value in the continuously changing inlet wind direction scenario is about twice that in the fixed inlet wind direction scenario. This is physically coherent since the continuously changing inlet wind direction, in the horizontal plane, forces a larger

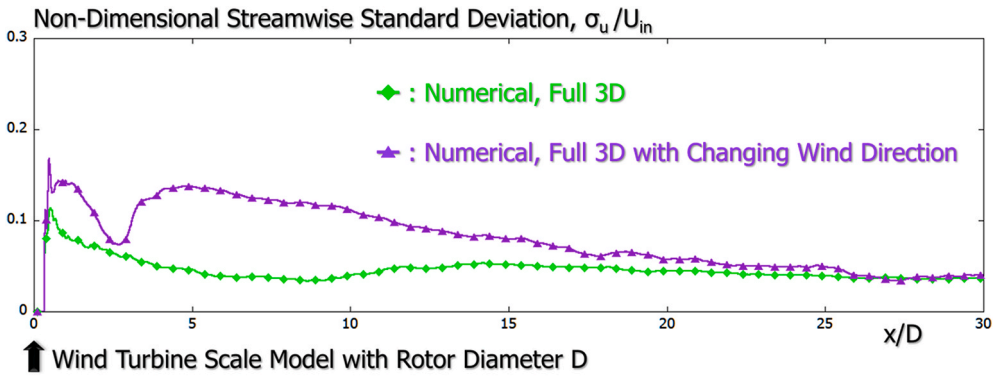


(a)

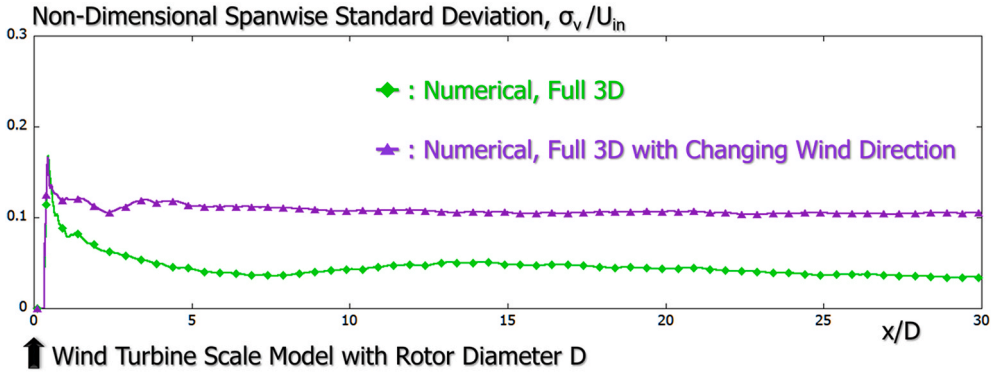


(b)

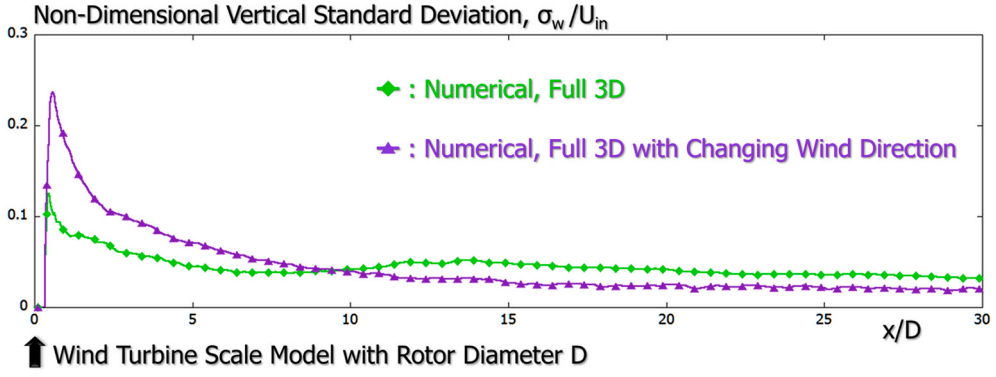


(c)

**Fig. 27.** Comparison of the distribution of the non-dimensional standard deviation, normalized by the average inlet wind velocity and computed over the second cycle (see Fig. 19), at the center of the wind turbine hub in three directions: (a) streamwise, (b) spanwise, and (c) vertical.

amplitude in the wake oscillation in the horizontal (x–y) plane, downstream of the wind turbine model. In the vertical direction shown on Fig. 27c, at x = 10D, the relationship of the magnitude between the two values is reversed. Namely, a spatially homogeneous and isotropic turbulence field is seemingly being formed in the swept area.

## 5. Conclusions

Considering that, under realistic atmospheric boundary layer conditions, the wind direction upstream of a utility-scale wind turbine is continuously changing, the wake characteristics behind the wind turbine are affected by this oscillating incoming flow. Therefore, understanding the effects of continuously changing wind direction on the wake characteristics of a wind turbine over flat terrain is necessary in designing wind farm layouts, including for offshore wind power plants.

Since the yaw angle threshold for activating the yaw control system is generally about ±15° in utility-scale wind turbines, the wake characteristics of a wind turbine was studied for continuously changing incoming flows with a yaw angle of ±10° in the horizontal (x–y) plane. Here, the velocity in the vertical (z) plane was zero. The increment angle was determined based on the results of our previous similar CFD-based sensitivity analysis (Uchida, 2020).

For this purpose, a computational fluid dynamics (CFD) approach using large-eddy simulations (LES) was adopted in the present study. An in-house LES-solver based on the actuator line (AL) aerodynamics technique was constructed in order to successfully capture the wake structure behind the wind turbine. Parallel computation based on a hybrid LES/AL model approach was performed with a new SX-Aurora

TSUBASA vector supercomputer.

First, experimental investigations on both a blade-only wind turbine scale model and a full 3D wind turbine scale model (isolated wind turbine), both with fixed inlet wind directions, were conducted, the latter including the nacelle and the tower, using the large closed-circuit atmospheric boundary wind tunnel at the Research Institute for Applied Mechanics (RIAM) of Kyushu University. Through a detailed comparison of the wind tunnel experimental and numerical results, the prediction accuracy of the in-house LES-solver was verified and validated for fixed inlet wind direction.

On the basis of the validation results obtained, and using the full 3D wind turbine scale model, the effects of the continuously changing inlet wind conditions on the wake characteristics in the near- and far-wake regions were numerically investigated. In addition, the effects of the wind turbine nacelle and tower on the wake characteristics were also investigated. The numerical results show that the most significant impact of the effects of the continuously changing wind direction was the rapid recovery of the mean velocity deficits in the wind turbine wake region. Further, at the x = 10D position (D is the rotor diameter) downstream of the wind turbine, the non-dimensional streamwise mean velocity was 0.93, which nearly matches the approaching flow speed, under an optimal tip speed ratio of 4.0, compared to the fixed wind direction scenario.

Further work includes a detailed study of the dynamic behavior of the wake behind a full 3D scale wind turbine model, along with studying the effect of the wake characteristics downstream wind turbines. On a more fundamental nature, the effect of increased turbulent mixing on the meandering of the wake remains a fundamental question that can be further studied. Regarding wind tunnel experimentation, it would be interesting to further study the effect of the confinement of the flow on the dynamics of the wind turbine wake. Finally, in application to wind power production, it would be interesting to study the behavior of wind turbine wakes subject to oscillating incoming wind conditions (periodic or random oscillations), but with yaw correction of the wind turbine to compensate for the variation in the angle of the incoming wind.

## CRediT authorship contribution statement

**Takanori Uchida:** Project administration, Conceptualization, Methodology, Software, Figure preparation, Formal analysis, Writing–original draft, preparation. **Yves Gagnon:** Supervision, Writing–review & editing, Investigation, Formal analysis.

## Declaration of competing interest

The authors declare that they have no known competing financial interests or personal relationships that could have appeared to influence the work reported in this paper.

## Acknowledgment

A part of this work is supported by Adaptable and Seamless Technology transfer Program through Target-driven R&D (A-STEP) from Japan Science and Technology Agency (JST) Grant Number JPMJTR211C.

## References

Abdelsalam, A.M., Boopathi, K., Gomathinayagam, S., Hari Krishnan Kumar, S.S., Ramalingam, V., 2014. Experimental and numerical studies on the wake behavior of a horizontal axis wind turbine. J. Wind Eng. Ind. Aerod. 128, 54–65.

Abkar, M., Porté-Agel, F., 2015. Influence of atmospheric stability on wind-turbine wakes: a large-eddy simulation study. Phys. Fluids 27 (3), 035104.

Abraham, A., Dasari, T., Hong, J., 2019. Effect of turbine nacelle and tower on the near wake of a utility-scale wind turbine. J. Wind Eng. Ind. Aerod. 193, 103981.

Aitken, M.L., Banta, R.M., Pichugina, Y.L., Lundquist, J.K., 2014a. Quantifying wind turbine wake characteristics from scanning remote sensor data. J. Atmos. Ocean. Technol. 31 (4), 765–787.

Aitken, M.L., Kosović, B., Mirocha, J.D., Lundquist, J.K., 2014b. Large eddy simulation of wind turbine wake dynamics in the stable boundary layer using the weather research and forecasting model. J. Renew. Sustain. Energy 6 (3), 033137.

Baker, R.W., Walker, S.N., 1984. Wake measurements behind a large horizontal axis wind turbine generator. Sol. Energy 33 (1), 5–12.

Braunbehrens, R., Segalini, A., 2019. A statistical model for wake meandering behind wind turbines. J. Wind Eng. Ind. Aerod. 193, 103954.

Chamorro, L.P., Porté-Agel, F., 2010. Effects of thermal stability and incoming boundary-layer flow characteristics on wind-turbine wakes: a wind-tunnel study. Boundary-Layer Meteorol. 136 (3), 515–533.

Churchfield, M.J., Lee, S., Michalakes, J., Moriarty, P.J., 2012. A numerical study of the effects of atmospheric and wake turbulence on wind turbine dynamics. J. Turbul. 13, N14.

Draper, M., Guggeri, A., Mendina, M., Usera, G., Campagnolo, F., 2018. A large eddy simulation-actuator line model framework to simulate a scaled wind energy facility and its application. J. Wind Eng. Ind. Aerod. 182, 146–159.

Foti, D., Yang, X., Shen, L., Sotiropoulos, F., 2019. Effect of wind turbine nacelle on turbine wake dynamics in large wind farms. J. Fluid Mech. 869, 1–26.

Göltenbott, U., Ohya, Y., Yoshida, S., Jamieson, P., 2017. Aerodynamic interaction of diffuser augmented wind turbines in multi-rotor systems. Renew. Energy 112, 25–34. https://doi.org/10.1016/j.renene.2017.05.014.

Hancock, P.E., Pascheke, F., 2014. Wind-tunnel simulation of the wake of a large wind turbine in a stable boundary layer: part 2, the wake flow. Boundary-Layer Meteorol. 151 (1), 23–37.

Hewitt, S., Margetts, L., Revell, A., 2018. Building a digital wind farm. Arch. Comput. Methods Eng. 25, 879–899.

Inagaki, M., Kondoh, T., Nagano, Y., 2005. A mixed-time-scale SGS model with fixed model-parameters for practical LES. ASME. J. Fluids Eng. January 127 (1), 1–13. https://doi.org/10.1115/1.1852479.

Iungo, G.V., Porté-Agel, F., 2014. Volumetric lidar scanning of wind turbine wakes under convective and neutral atmospheric stability regimes. J. Atmos. Ocean. Technol. 31 (10), 2035–2048.

Keck, R.E., de Maré, M., Churchfield, M.J., Lee, S., Larsen, G., Aagaard, M.H., 2014. On atmospheric stability in the dynamic wake meandering model. Wind Energy 17 (11), 1689–1710.

Machefaux, E., Larsen, G.C., Koblitz, T., Troldborg, N., Kelly, M.C., Chougule, A., Hansen, K.S., Rodrigo, J.S., 2016. An experimental and numerical study of the atmospheric stability impact on wind turbine wakes. Wind Energy 19 (10), 1785–1805.

Magnusson, M., Smedman, A.S., 1999. Air flow behind wind turbines. J. Wind Eng. Ind. Aerod. 80 (1), 169–189.

Matsumiya, H., Kogaki, T., Takahashi, N., Iida, M., Waseda, K., 2011. Development and experimental verification of the new MEL airfoil series for wind turbines. In: Proceedings of Japan Wind Energy Symposium, vol. 22, pp. 92–95. https://www.jstage.jst.go.jp/article/jweasympo1979/22/0/22_0_92/_article/-char/en.

Ministry of Economy, Trade and Industry (METI), 2020. Green Growth Strategy through achieving carbon neutrality in 2050. Formulated. https://www.meti.go.jp/english/press/2020/1225_001.html.

Mirocha, J.D., Rajewski, D.A., Marjanovic, N., Lundquist, J.K., Kosović, B., Draxl, C., Churchfield, M.J., 2015. Investigating wind turbine impacts on near-wake flow using profiling lidar data and large-eddy simulations with an actuator disk model. J. Renew. Sustain. Energy 7 (4), 043143.

Mo, J.O., Choudhry, A., Arjomandi, M., Lee, Y.H., 2013. Large Eddy Simulation of the wind turbine wake characteristics in the numerical wind tunnel model. J. Wind Eng. Ind. Aerod. 112, 11–24.

Ohya, Y., Karasudani, T., 2010. A shrouded wind turbine generating high output power with wind-lens technology. Energies 3, 634–649. https://doi.org/10.3390/en3040634.

Porté-Agel, F., Bastankhah, M., Shamsoddin, S., 2020. Wind turbine and wind-farm flows: a review. Boundary-Layer Meteorol. 174, 1–59.

Porté-Agel, F., Wu, Y.T., Chen, C.H., 2013. A numerical study of the effects of wind direction on turbine wakes and power losses in a large wind farm. Energies 6, 5297–5313.

Santoni, C., Carrasquillo, K., Arenas, I., Leonardi, S., 2017. Effect of tower and nacelle on the flow past a wind turbine. Wind Energy 20 (12), 1927–1939.

Sedaghatizadeh, N., Arjomandi, M., Kelso, R., Cazzolato, B., Ghayesh, M.H., 2018. Modelling of wind turbine wake using large eddy simulation. Renew. Energy 115, 1166–1176. https://doi.org/10.1016/j.renene.2017.09.017.

Sedaghatizadeh, N., Arjomandi, M., Kelso, R., Cazzolato, B., Ghayesh, M.H., 2016. Effect of wall confinement on a wind turbine wake. In: 20th Australasian Fluid Mechanics Conference, Perth Australia, pp. 5–8. Dec 2016.

Segalini, A., Inghels, P., 2014. Confinement effects in wind-turbine and propeller measurements. J. Fluid Mech. 756, 110–129.

Sessarego, M., Shen, W.Z., van der Laan, M.P., Hansen, K.S., Zhy, W.J., 2018. CFD simulations of flows in a wind farm in complex terrain and comparisons to measurements. Appl. Sci. 8, 788–809.

Tian, W., Ozbay, A., Hu, H., 2018. An experimental investigation on the aeromechanics and wake interferences of wind turbines sited over complex terrain. J. Wind Eng. Ind. Aerod. 172, 379–394.

Uchida, T., 2020. Effects of inflow shear on wake characteristics of wind turbines over flat terrain. Energies 13 (14), 3745.

Uchida, T., Li, Graham, 2018. Comparison of RANS and LES in the prediction of airflow field over steep complex terrain. Open J. Fluid Dynam. 8, 286–307.

Uchida, T., Maruyama, T., Ohya, Y., 2011b. New evaluation technique for wtg design wind speed using a CFD-model-based unsteady flow simulation with wind direction changes. Model. Simulat. Eng. Article ID: 941870.

Uchida, T., Ohya, Y., Sugitani, K., 2011a. Comparisons between the wake of a wind turbine generator operated at optimal tip speed ratio and the wake of a stationary disk. Model. Simulat. Eng. Article ID: 9749421.
Uchida, T., Takakuwa, S., 2019. A large-eddy simulation-based assessment of the risk of wind turbine failures due to terrain-induced turbulence over a wind farm in complex terrain. Energies 12, 1925.
Uchida, T., Taniyama, Y., Fukatani, Y., Nakano, M., Bai, Z., Yoshida, T., Inui, M., 2020. A new wind turbine CFD modeling method based on a porous disk approach for practical wind farm design. Energies 13 (12), 3197.
Uchida, T., Yoshida, T., Inui, M., Taniyama, Y., 2021. Doppler lidar investigations of wind turbine near-wakes and LES modeling with new porous disc approach. Energies 14, 2101.
Whale, J., Anderson, C.G., Bareiss, R., Wagner, S., 2000. An experimental and numerical study of the vortex structure in the wake of a wind turbine. J. Wind Eng. Ind. Aerod. 84, 1–21.
Wu, Y.T., Porté-Agel, F., 2012. Atmospheric turbulence effects on wind-turbine wakes: an LES study. Energies 5 (12), 5340–5362.
Zhang, W., Markfort, C.D., Porté-Agel, F., 2013. Wind-turbine wakes in a convective boundary layer: a wind tunnel study. Boundary-Layer Meteorol. 146 (2), 161–179.